Magnetic Characterization of Fine Sediment in the Solo Basin Indonesia

Budi Legowo[1,*], Anti Fatkhul Qoiriah[1], Artono Dwijo Sutomo[1], Shandiyano Putra[1], Wiwit Suryanto[2] & Budi Purnama[1]

[1]Physics Department, Universitas Sebelas Maret, Jalan Ir. Sutami 36A, Kentingan, Surakarta 57126, Indonesia
[2]Physics Department, Gadjah Mada University, Bulaksumur, BLS21, Yogyakarta 55281, Indonesia
*E-mail: pakbeel@staff.uns.ac.id

Abstract. The magnetic characteristics of fine sediment samples from the Solo Basin are reported in this paper. Magnetic fine sediment was identified by magnetic susceptibility mapping based on sampling of 182 points. Then, a depth analysis (on 7 selected sampling points) was performed using X-ray fluorescence spectrometry, which showed an iron oxide content of up to 55.42%, while X-ray diffractometry confirmed magnetite minerals with crystallite size ≤100 nm. Further, the vibrating sample magnetometry results verified the magnetic characteristics under a single-domain configuration. The characteristic magnetic susceptibility map showed that there is a lithogenic effect on sediment in the Solo Basin. In addition, anthropogenic activities seem to play a pivotal role in distributing magnetic materials.

Keywords: *fine sediment; iron oxide; magnetic susceptibility; single domain; solo basin.*

1 Introduction

The Solo Basin is located in the central depression zone of Java, Indonesia. It is an active sedimentary basin with a fluvial environment, receiving sediment supply from adjacent active volcanoes (including Merapi, Merbabu, Lawu, and Old Lawu volcanoes) and the Kendeng Zone (Figure 1). Moreover, the Solo Basin is known to have been formed in the Late Pleistocene to Holocene and it consists of Alluvium (Qa), Older Alluvium (Qt), Merapi Volcanic Rock (Qvm), and Lawu Volcanic Rock (Qvl) sediment. Alluvium sediment usually consists of loose clay, silt, sand, or gravel that has undergone a sedimentation process at the bottom of the river. Merapi volcanic rock is a rock that was released by the process of volcanism. The process of volcanism in question is a mountain eruption. The eruption releases pyroclastic materials. These can be divided into two types, namely materials from pyroclastic deposit and from pyroclastic flow. Pyroclastic deposit is a pyroclastic deposition process found somewhere either around or far from the mountain. Pyroclastic flow comes out of the mouth of the volcano. The Solo Basin, which covers an area of 16,000 km^2, is filled with water originating from the longest and largest river in Java, Bengawan Solo River,

Received June 23th, 2022, Revised January 9th, 2023, Accepted for publication November 30th, 2023
 ISSN: 2337-5760, DOI: 10.5614/j.math.fund.sci.2023.55.2.1

which originates from the Sewu mountains in the west to the south and stretches to the Java Sea and has a length of ±600 km [1-4].

In addition, there is one of the world's most important archaeological sites, the Sangiran Dome, which is the main stratigraphic window for Pleistocene deposits in the Solo Basin [5-7]. The Sangiran Dome is formed from four formations, namely the Puren Formation, the Sangiran Formation, the Bapang Formation, and the Pohjajar Formation. The Pohjajar Formation is the youngest among them. The oldest formation is the Puren Formation. The Puren Formation is squeezed by the Sangiran Formation and it can be divided into three sections, namely, lower, middle, and upper. All sections are filled with volcanic material originating from Mount Lawu, Mount Merbabu, and Mount Merapi. Nowadays, the presence of these volcanoes supports the existence of the Solo Basin due to parent rock that undergoes a weathering process and is carried away by transport media such as water and wind. Further, a final process of sedimentation will occur in the basin zone [8]. Among various magnetic minerals produced by magnetic rocks, magnetites include minerals that are easy to store and resistant to weathering [9-11]. Sediment in the Solo Basin comes from erosion processes originating from the Merapi, Merbabu, and Lawu volcanoes, the Kendeng Zone, and the Sangiran Dome [2,3,12]. Moreover, the presence of metallic iron oxides indicates that lithogenic processes contribute to the magnetic mineral formation in the sediment [13-15].

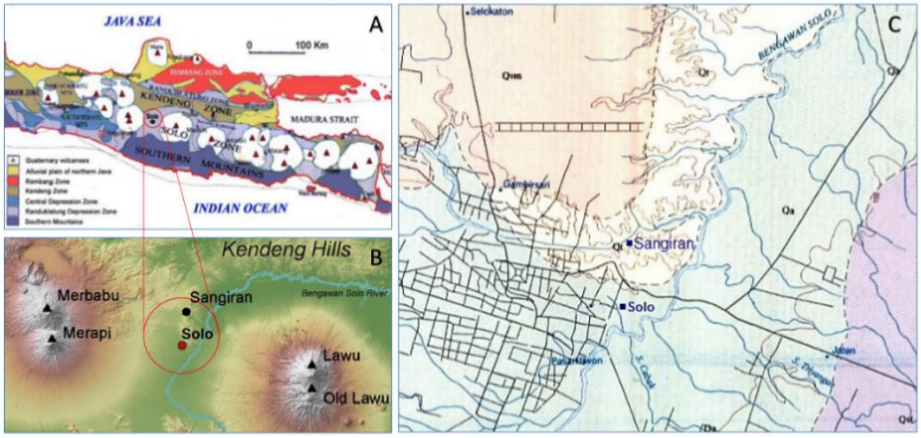

Figure 1 **A** Physiography of Java Island. The Solo Zone is formed by a modern volcanic belt extending in a west-east direction in the middle of Java Island [16]. **B** Solo Basin (research location) – including the Sangiran Dome – bordering the Kendeng Zone to the north, a hilly area composed of deep-sea sediment [7]. **C** Simplified from a geological map of the Surakarta–Giritontro Quadrangles. The Solo Basin was formed in the Late Pleistocene to Holocene and consists of Alluvium (Qa), Older Alluvium (Qt), Merapi Volcanic Rocks (Qvm) and Lawu Volcanic Rocks (Qvl) sediment [17].

Fine deposits from the lithogenic process include sulfides and iron oxides such as magnetites [18-20]. Therefore, the source of the sediment is crucial for understanding the evolutionary process of an area [20]. Notably, the type of volcano defines the magnetic minerals contained in the rock and sediment [21]. Magnetic minerals are very dependent on the metal concentration contained in the sample. The more metal the samples they contain, the more magnetic they are. Vice versa, the lower the metal concentration in the rock, the less magnetic the minerals. The presence of ferromagnetic magnetites can be studied using magnetic susceptibility measurements [22-24]. A higher magnetic susceptibility value of a material indicates that the material only accepts an external magnetic field with great difficulty. Differences in lithographic conditions indicate differences in rock magnetic characteristics associated with differences in rock recrystallization processes [23].

Magnetic studies of rocks and analysis of their magnetic characteristics have developed rapidly and especially the magnetic susceptibility of rocks has now become one of the fundamental characteristics of rocks [25-46]. Initially, magnetic characteristics were identified from the source of the magnetic rock. From a theoretical viewpoint, it is known that magnetic minerals are the result of solid-solution processes of titanomagnetite, ilmenohematite, and pseudobrookite [39]. Therefore, the process of rock formation is an important factor that must be considered. The relationship between the direction of magnetic anisotropy and the orientation of crystal formation, especially the formation of single crystals, has been confirmed [25]. In contrast, the orientation of magnetic anisotropy indicates the direction of the lava flow in the volcano [32]. The hydration or dehydration process partially changes titanian clinohumite to ilmenite (+magnetite) [28]. Furthermore, weather and transport processes are crucial in distributing magnetic minerals [19,36]. Lithogenic and anthropogenic factors also play a role in the distribution of fine sediment [26]. It has also been reported that both technological activity [27] and contamination play a role in the evolution of rock magnetic zones [28,46,24].

Here, the identification of magnetic minerals, which support lithogenic, pedogenic, and anthropogenic origins, through susceptibility measurement was the easiest procedure [32]. Moreover, the ratio of the susceptibility measurements of two frequencies, namely low and high frequencies, is sufficient to characterize the reversal-magnetization mode of the magnetic mineral being measured [33]. Lithogenic magnetite particles are present as pseudo/multi-domains with large-enough particle sizes, while pedogenic fine-grained particles are present as single domains or superparamagnetic particles [37]. Therefore, the identification of magnetic minerals can give an indication of the period of rock formation as well as the environmental quality due to anthropogenic activities. Meanwhile, the

representation of magnetic properties may be expressed from the magnitude of the susceptibility measurement in a certain area.

In this study, we studied the magnetic properties and geochemical characteristics of fine sediment samples from the Solo Basin. The element or metal oxide content of the sediment was evaluated to confirm the presence of magnetic minerals as a source of modification of the measured magnetic susceptibility magnitude. Magnetic susceptibility magnitude distribution mapping was performed to represent the magnetic properties of the fine sediment as well as the parent rock formation in the Solo Basin.

2 Materials and Methods

2.1 Mineral Content Analysis

Identification of magnetic property characteristics was carried out on sediment samples from the Solo Basin. The samples came from debris of volcanic material originating from Merapi volcano, Merbabu volcano, and Lawu volcano. Representative samples were taken based on different topographical structures and land uses, so they could represent the entire research site.

The obtained sediment samples were dried using an oven at 110°C for 48 hours. Furthermore, the samples were mashed by ball milling for 3 hours to produce fine granules [11]. Thereafter, the sample was filtered to separate coarse grains from fine grains. The obtained sediment samples were then separated between non-magnetic and magnetic minerals using a permanent magnet [8,47]. X-ray fluorescence (XRF) was used to determine the contents of the sediment. Furthermore, Fourier transform infrared (FTIR) spectroscopy was used to evaluate the appearance of hydrocarbon and oxide bonds, especially metal-oxide bonds. X-ray diffractometry (XRD) was used to analyze the crystalline structure following identification of the types of minerals in the fine sediment samples. Vibrating sample magnetometry (VSM) at room temperature was used to identify the magnetic properties of the fine sediment samples [9,15,48-50].

2.2 Magnetic Properties: Magnetic Susceptibility Mapping

Direct measurements were taken in the field using a susceptibility cappameter with code KT-5. This was done for the process of collecting samples for further testing. The frequency used was 10 kHz with a sensitivity of 1×10^{-5} and measuring ranges from -999 to 9999×10^{-3} SI [21,49]. Figure 2 shows a map of the magnetic susceptibility research location with a total of 184 measurement points. The interval between points was 500 meters. For each individual sampling point, the magnetic susceptibility was measured for 15 repetitions. The blue dots

are the sediment sampling points selected for further physical property characterization.

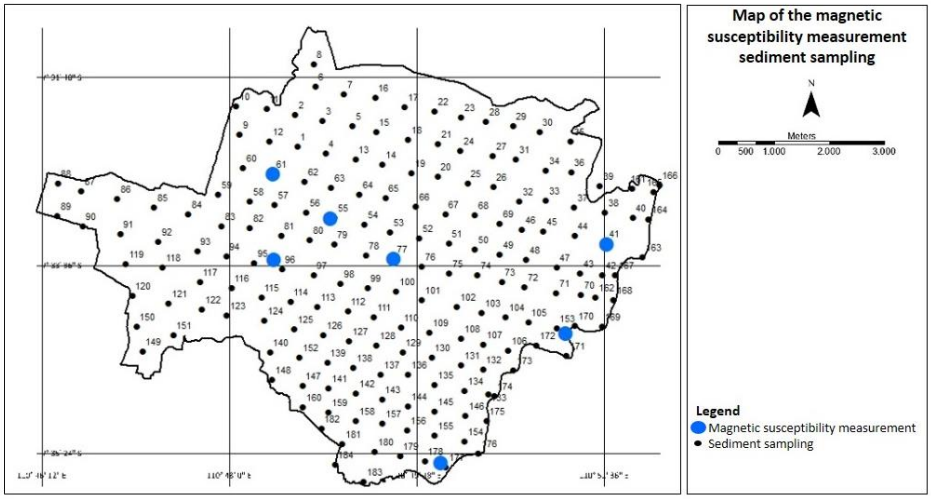

Figure 2 Map of surface sediment magnetic susceptibility measurements in the Solo Basin area and sediment sampling locations for further physical property characterization.

3 Results and Discussion

3.1 Solo Basin Sedimentation

The sampling location was within the limits of 110º45′15″E–110º45′35″E and 7º36′00″S–7º56′00″S. Figure 1B shows topographic and cross-sectional contour maps of the Solo Basin, with Mount Lawu (3,265 masl) and Mount Merapi (2,911 masl) bounding the east and west sides, respectively. On the north side, there is the Kendeng Zone and the Sagiran Dome, which have been disrupted since the end of the Pleistocene [7,12]. Figure 1C shows most of the geological formations of the Solo Basin formed by alluvium composed of clay, mud, silt, sand, gravel, pebble, and cobble. Viewed from several sides, the northern part is dominated by old alluvium formed from conglomerate rock, sandstone, silt, and clay. The west to east sides have volcanic breccia, lava, and tufa rock formations, which originate from the volcanoes of Merapi and Lawu. [16,17]. Thus, the magnetic sediment that occurs in the Solo Basin should be supported by volcanic parent rock.

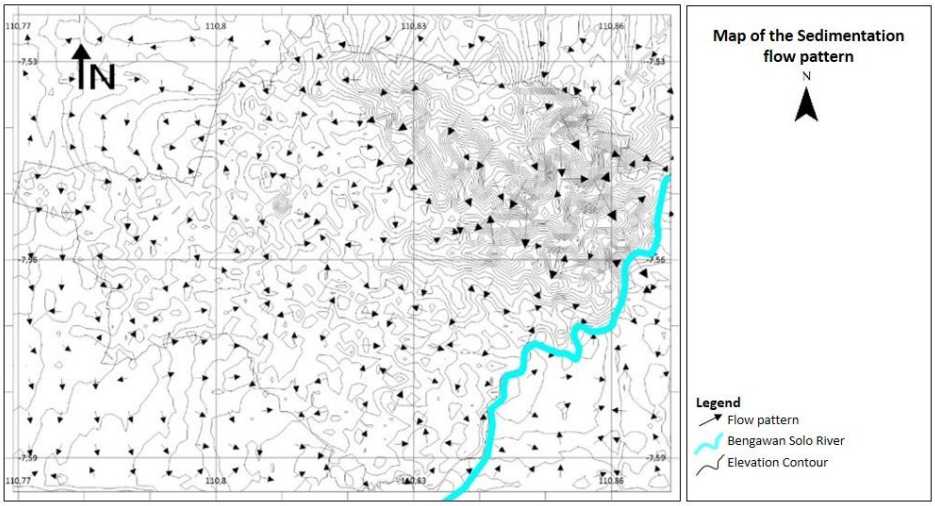

Figure 3 Sedimentation flow pattern of the Solo Basin (no scale).

Regarding the above topographic profile, sedimentation should be more concentrated in the lower areas. Moreover, sedimentation flow patterns, which indicate the magnetic mineral content at different slope positions, can be estimated [14,46].

Figure 3 shows the sedimentation flow pattern of Solo Basin. The flow pattern is toward the lower east side and the Bengawan Solo River (indicated by a blue line). The north-northeast region has a higher topographic structure than the other regions. Meanwhile, the south-east region has a lower topography than the other regions. Thus, the south–east region has large sedimentation compared with the other regions. The southern region is included in the category of land prone to flooding (flood plain) because there is fluvial sediment from the Bengawan Solo River [2,4,51].

3.2 Analysis of the Sediment Content of Solo Basin Samples

The content analysis of sediment samples at the surface and a depth of 30 cm was performed using XRF characterization. The identified minerals are presented in Table 1, where the concentrations are expressed in percentage (%). The various sediment contents cannot be separated from the parent material, which has undergone weathering and sedimentation. The oxide bond content in Table 1 corresponds to the oxide bond content found in the Merapi volcano. In the study of weathering of the pyroclastic deposits of the Merapi volcano, oxide bonds are also found in the sediments from the Solo Basin, namely, Fe–O, Si–O, Al–O, Ca–O, Ti–O, K–O, P–O, and Mn–O, where these materials are compositions of

andesite and basaltic rocks [52]. Meanwhile, the pyroclastic material of the Merapi volcano in the 2010 eruption was dominated by the mineral plagioclases [53].

Tabel 1 (a) Composition of sediment samples taken from the surface.

Compound	Compound concentration at location (%)						
	no. 41	no. 55	no. 61	no. 77	no. 95	no. 171	no. 177
Fe–O	44.93	38.12	33.35	32.10	43.28	51.04	46.10
Si–O	28.70	31.20	34.50	33.00	30.50	28.10	30.80
Al–O	9.10	9.60	11.00	9.70	12.00	9.30	9.90
Ca–O	8.78	13.60	11.50	16.50	6.46	3.69	5.99
Ti–O	4.28	3.85	2.69	3.02	4.91	4.91	3.84
K–O	1.29	1.55	1.95	1.56	1.16	0.62	0.96
Mn–O	0.59	0.50	0.45	0.50	0.45	0.46	0.46
Eu–O	0.51	0.40	0.49	0.45	0.46	0.48	0.48
P–O	0.73	-	0.56	1.00	0.61	0.53	0.56
V–O	0.27	0.27	0.17	0.18	0.29	0.35	0.24
Re–O	0.27	0.27	0.25	0.07	0.20	0.20	0.20
Pb–O	-	0.26	-	-	-	-	-
Sr–O	0.20	-	0.25	0.25	-	-	-
Hg–O	-	-	-	0.17	-	-	-
Rb–O	0.16	0.10	-	-	0.14	0.16	0.15
Cr–O	0.10	0.08	0.12	0.09	0.08		0.09
Zn–O	0.08	0.06	0.13	0.16	0.04	0.04	0.07
Mo–O	-	0.08	2.90	-	-	-	-
Cu–O	0.07	0.06	0.09	0.09	0.06	-	0.07
Br	-	0.06	-	-	-	-	-

Research conducted in the Bengawan Solo River found that the dominant contents of the sediment were Fe–O, Si–O, Ti–O, Al–O, Ca–O, and P–O [9]. The Bengawan Solo River headwaters are at the foot of the Merapi and Southern volcanoes [2,3]. Thus, the sediment in the Solo Basin is compatible with the volcanic materials of the Merapi and Lawu volcanoes and sediment in the Bengawan Solo River.

In the transport stage of eroded volcanic materials from the Merapi and Lawu volcanoes to the Solo Basin, water is the dominant transport medium. The water source can be rainwater or river flows. The rate of erosion is proportional to the

increase in rainfall intensity and land slope steepness [51,54]. The largest river flow that transports materials from upstream to the Solo Basin is the Bengawan Solo River.

Table 1 (b) Composition of sediment samples taken from a depth of 30 cm.

Compound	Compound concentration at location (%)						
	no. 41	no. 55	no. 61	no. 77	no. 95	no. 171	no. 177
Fe–O	44.52	45.22	43.04	44.84	42.33	55.42	40.00
Si–O	29.90	28.80	32.60	30.90	30.80	23.80	36.30
Al–O	9.10	10.00	10.00	10.00	11.00	9.20	12.00
Ca–O	9.07	7.52	7.31	7.00	8.81	2.49	5.32
Ti–O	4.17	4.27	4.00	4.61	4.26	6.00	3.76
K–O	1.34	1.13	1.14	0.82	0.89	0.47	0.72
P–O	0.75	-	-	-	0.62	0.52	-
Mn–O	0.53	0.48	0.46	0.52	0.45	0.49	0.44
Eu–O	0.45	0.47	0.47	0.43	0.45	0.53	0.42
V–O	0.28	0.28	0.29	0.33	0.29	-	0.25
Re–O	0.28	0.20	0.22	0.23	0.26	0.20	0.20
Rb–O	0.15	0.15	0.14	0.16	0.15	0.18	0.13
Cr–O	0.09	0.86	0.08	0.07	0.07	0.10	0.08
Zn–O	0.09	0.27	0.10	0.09	0.05	0.06	0.04
Cu–O	0.07	0.08	0.08	0.06	0.06	0.05	0.05

3.3 Analysis of Oxide Groups in Solo Basin Sediment Samples

Figure 4 shows the FTIR curves of fine sediment samples taken from the surface and a depth of 30 cm. There is no significant difference between the FTIR patterns in the surface and 30-cm depth samples. The presence of metal oxides is predicted from the absorption curve that appears in the wavenumber range k = 372–464 cm^{-1}. The wavenumber values of the two variations indicate the general characteristics of metallic bond vibrations (Fe–O). This is in accordance with previous studies, in which Fe–O bond vibration occurred around the wavenumber range of 461–475 cm^{-1} [52] and metallic bond vibration (Fe–O) occurred at an absorption wavelength of 377 cm^{-1} [48]. Thus, the sediment samples, both taken from the surface and a depth of 30 cm, have characteristic magnetic properties.

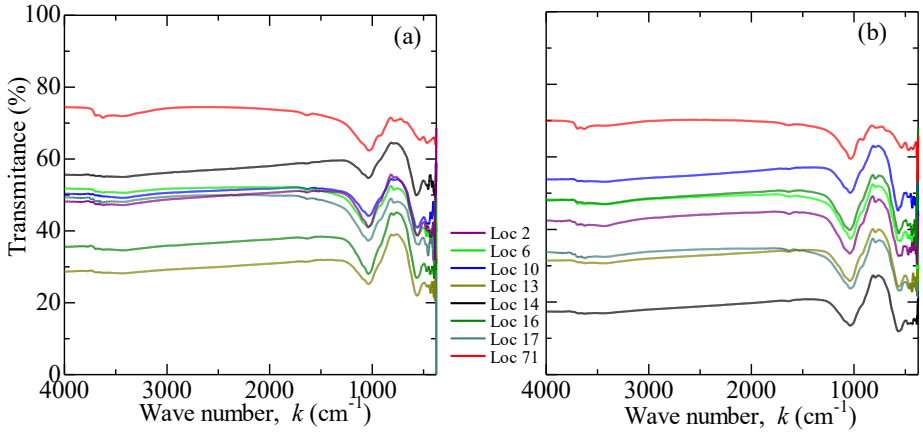

Figure 4 Results of FTIR characterization of sediment samples taken from (a) the surface and (b) 30-cm depth.

3.4 Analysis of Crystal Structure of Solo Basin Sediment Samples

Figures 5(a) and (b) show the patterns obtained from XRD characterization of the surface and the 30-cm depth samples. The XRD plots of the surface and 30-cm depth samples are relatively the same. The XRD pattern results are suitable for RRUFF ID R060191, namely, magnetite (Fe_3O_4). In addition, some XRD patterns show conformity with anorthite ($Ca(Al_2Si_2O_8)$), albite ($Na(AlSi_3O_8)$), and cristobalite (SiO_2).

The obtained results agree with previous research, in which sediment originating from the parent volcanic material of the Merapi volcano contained anorthite and albite minerals, which are plagioclases minerals [53]. Researching the Old Lawu volcano [56] found several minerals, including albite and cristobalite. Cristobalite minerals were also found in the Merapi volcano, which were classified as plagioclases of crystalline minerals [52]. Plagioclases are the main minerals that comprise the Merapi volcano rock [8,56]. Magnetite minerals, which are not significantly affected by weathering were also found in Merapi volcano and Bengawan Solo River sediment samples [9,16].

To determine the distribution of particle sizes, assuming the fine sediments have particle sizes in the order of nanometers, the crystallite size is proportional to the average particle size of the fine sediments of the Solo Basin. Using the Debye–Scherrer equation, $D = \frac{k\lambda}{\beta \cos\theta}$ [49], and calculations at the strongest peak, the crystallite size D is summarized in Table 2.

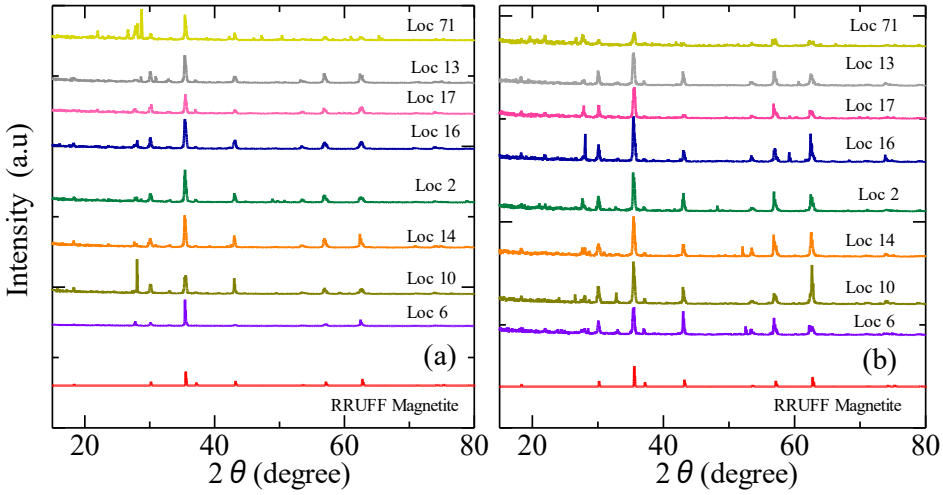

Figure 5 XRD patterns of fine sediment samples taken from (a) the surface and (b) 30-cm depth.

Table 2 Calculation of crystallite size *D* for sediment samples taken from the surface and a depth of 30 cm.

Location	D (nm) surface	D (nm) 30-cm depth
no. 41	141.31 ± 0.63	46.21 ± 0.23
no. 55	96.76 ± 0.65	103.94 ± 0.43
no.61	69.29 ± 0.31	83.22 ± 0.36
no. 77	104.05 ± 0.43	104.04 ± 0.43
no. 95	104.01 ± 0.43	17.33 ± 0.16
no. 171	83.34 ± 0.36	53.01 ± 0.27
no. 177	92.15 ± 0.53	112.37 ± 0.64

For all seven selected sampling points, the distribution of crystallite size *D* in the surface and 30-cm depth samples did not show a significant difference, i.e., it ranged from 17.33 to 104.05 nm. The crystallite size determines the appearance of the magnetic characteristics, especially regarding the reversal magnetization mode.

3.5 Analysis of Magnetic Properties of Solo Basin Sediment Samples

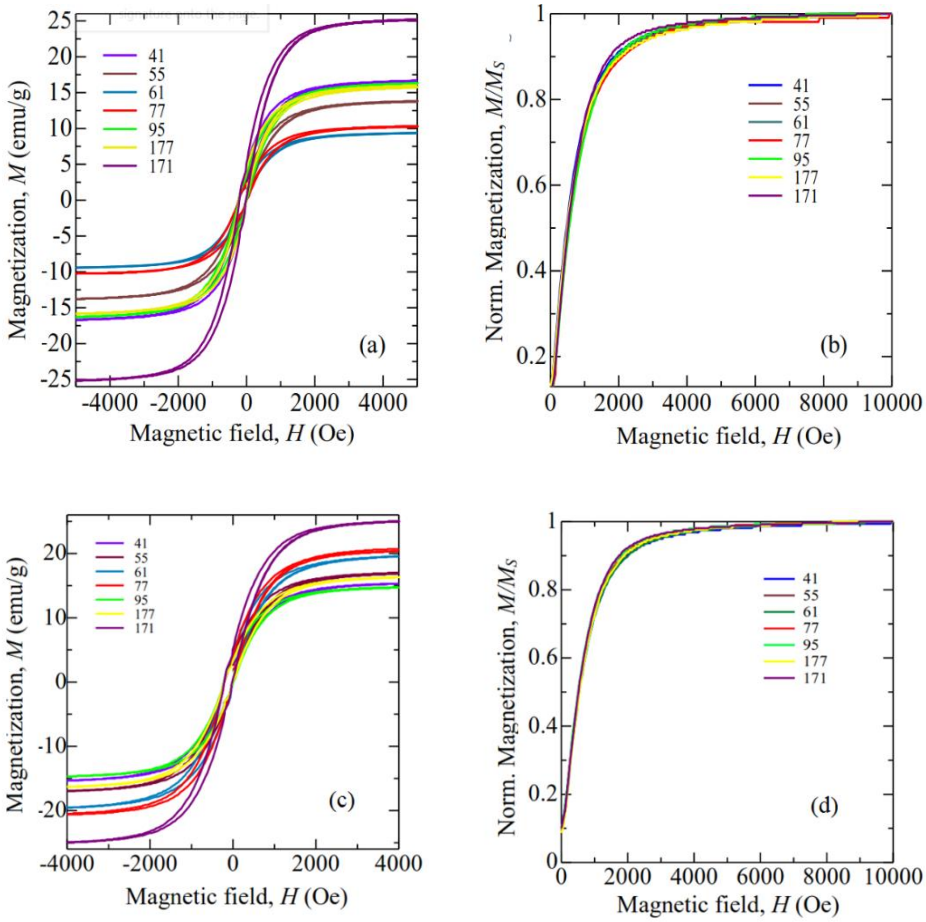

Figure 6 Hysteresis curves and normalized magnetizations of fine sediment samples taken from (a, b) the surface and (c, d) 30-cm depth.

Figure 6 shows the hysteresis curve and normalized magnetization at room temperature for fine sediment samples taken from the surface and 30-cm depth. The curves have an almost symmetric reverse order when applied to the magnetic field or when the magnetic field is removed. The hysteresis curves in Figures 6 (a) and (c) have a narrow area, which indicates the energy required for the magnetization process. The narrow area of the hysteresis curves indicates the presence of soft magnetic materials from the Solo Basin's deposit, namely, magnetites, as discussed above. Typical coercive values in

the range of 100 to 130 Oe for both the surface and the 30-cm depth samples further confirm that the magnetite mineral distribution is insensitive to weather changes [57].

Figures 6 (b) and (d) show the magnetization curve from the demagnetized state to the saturated magnetization state. When the magnetic field *H* is greater than 4000 Oe, a saturation state of magnetization is reached, i.e., the minimum magnetic field required to reach the magnetite saturation state. Further, all samples show the same magnetization pattern: the magnitude of magnetization suddenly or spontaneously reaching a saturation state. This indicates a single domain (SD) is realized for the entire sample [46,58,22]. This result is also supported by the nonzero magnetization in the initial state, namely, the zero field, H = 0. This can be explained as follows. From a theoretical perspective, the magnetic anisotropy and particle size of a material determine the magnetization realization type, either SD or multidomain. For nanoparticles, the particle size can be represented by the crystallite size. Calculations with the XRD data confirmed that all samples had a maximum crystallite size of ~100 nm, which is the limit size of SD realization.

3.6 Analysis of the Distribution of Magnetic Susceptibility Magnitudes in the Solo Basin

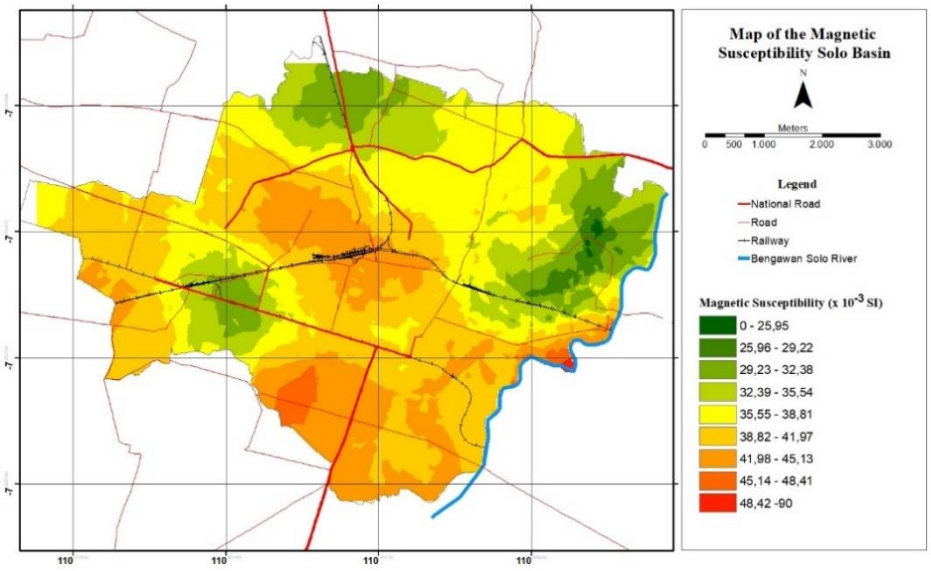

Figure 7 Distribution map of magnetic susceptibility (χ) for the Solo Basin surface.

Figure 7 shows a distribution map of the magnetic susceptibility (χ) of the surface sediment in the Solo Basin. From the figure, the northern area has a lower susceptibility magnitude, (0.90–3.80) × 10^{-2} SI, than the southern area of the Solo Basin, (3.90–6.50) × 10^{-2} SI. This correlates with the area's topography. The XRF results confirmed that Fe–O (magnetite) was more commonly found in areas with a low topography. The measured value of high magnetic susceptibility indicates the presence of more magnetic sources or high magnetizing strength. However, in areas with a relatively low topography, low magnetic susceptibility was found, i.e., less than 3.50 × 10^{-2} SI. These areas are known to have a relatively larger human population than others. These results confirm the anthropogenic support for the distribution of magnetic fine sediment in the Solo Basin area. We compared the pyroclastic flow data from the eruption of Mount Lawu with data from studies carried out on fine sediment carried out along the Bengawan Solo River. The magnetic susceptibility values had the same characteristics, ranging from 74.40–5,262.10 x 10^{-8} m^3/kg measured with Barthington MS2 with sensor B (mass) [59].

3.7 Scanning Electron Microscope Analysis

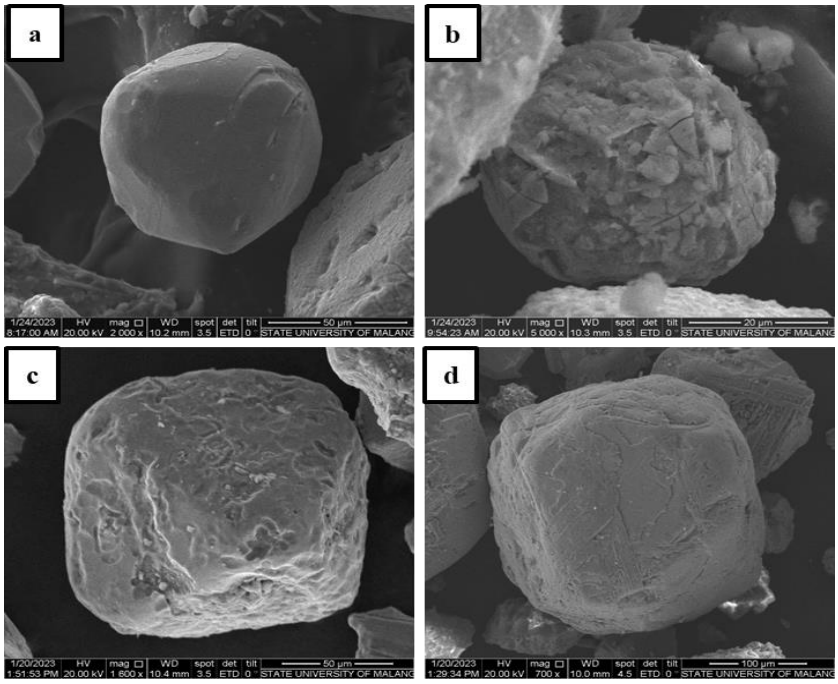

Figure 8 Scanning electron microscope (SEM) morphological forms, in sequence from code no. 41, no. 55, no. 61 and no. 77. a,c,d) Phases from lithogenic to autogenic; b) autogenic grain.

There are four different item forms, in sequence from a) Code no. 41; b) Code no.55; c) Code no.61; d) Code no.77. The four types of grain obtained can be divided into two types of grain, autogenic and lithogenic. Autogenic is sediment that is influenced by the activities of living things, such as burning and dumping industrial waste, while lithogenic is the formation of purely natural sediment such as weathering on rocks due to rain and river water flow. Autogenic grains have very different shapes compared to lithogenic grains. There is a phase change in the form of imperfect granules, or it could be said that there are many autogenic processes that have an influence along the Bengawan Solo River, resulting in the shape of the granules becoming uneven. The shapes of grains found in the environment are very diverse, ranging from long, cubic, circular to completely irregular. In the samples taken this time, the grains dominantly had circular shapes. Circular-shaped items indicate that the samples taken were formed by anthropogenic processes that may occur due to the burning of fossils from motorized vehicles, fly ash, and roadside sediment. The size of the magnetic grains obtained ranged from 20 to 100 μm. This size is included in the fine grain category, referring to samples that have been studied previously in roadside dust [60], flying dust [61], and soil [62].

4 Conclusion

In this paper, a study of the magnetic characteristics of fine sediments from the Solo Basin was discussed. The presence of fine magnetic sediment was identified by magnetic susceptibility mapping. Further, an XRF analysis was performed, which showed an iron oxide content of up to 55.42%, whereas XRD confirmed the presence of magnetite minerals with crystallite size ≤ 100 nm. The VSM results verified the magnetic characteristics in the presence of an SD magnetic configuration in the fine sediment from the Solo Basin. The magnetic susceptibility map showed that there is a lithogenic effect on sediment in the Solo Basin. In addition, anthropogenic activities play a key role in distributing magnetic materials.

Acknowledgment

This research was funded by DIPA of Universitas Sebelas Maret of the Republic of Indonesia (Hibah PDD PNBP Contract No. 260/UN27.22/HK.07.00/2021).

References

[1] Sartono, S., *Genesis Solo Terraces*, Modern Quaternary Research in Southeast Asia, **2**, pp. 1-21, 1976.
[2] JICA, *Upper Solo River Improvement Project*, Japan's ODA, Japan, 2002.

[3] Umboro, L., Ealisa, L., Hera, W. & Z.F., *Flood Assessment of Bengawan Solo River,* APRN Journal of Engineering and Applied Sciences, **11**(24), pp. 14443-14450, 2016.

[4] Senjaya, T., Yudianto, D., Yuebo, X. & Adidarma, W.K., *Application of TRMM in the Hydrological Analysis of Upper Bengawan Solo River Basin,* Journal of the Civil Enginerring Forum, **6**(3), pp. 309-318, 2020.

[5] Larick, R., Ciochon, R.L., Zaim, Y., Sudijono, Suminto, Rizal, Y. ... & Heizler, M., *Early Pleistocene 40 Ar/39Ar Ages for Bapang Formation Homonis, Central Jawa, Indonesia,* The Proceedings of the National Academy of Sciences, **98**(9), pp. 4866-4871, 2001.

[6] Arthur, B.E., Adrian, M.K., Scott, C.J., Roy, L., Yahdi, Z., Yan, R., Russell, C.L., Stephanie, T.S.A., Daniel, M., Suminto & Sutikno, B., *Way Out of Africa: Early Pleistocene Paleoenvironments Inhibied by Homo Erectus in Sangiran, Java,* Journal of Human Evolution, **56**(1), pp. 11-24, 2009.

[7] Berghuis, H.W., Veldkamp, A., Adhityatama, S., Hilgen, S.L., Sutisna, I., Barianto, D.H. ... & Joordens, J.C., *Hoominin Homelands of East Java: Revised Stratigraphy and Landscape Resonstructions for Plio-Pleistocen Trinil,* Quarternary Science Reviews, **260**, pp. 1-27, 2021.

[8] Hariyono, E. & Liliasari, S., *The Characteristics of Volcanic Eruption in Indonesia,* in Volcanoes - Geological and Geophysical Setting, Theoretical Aspects and Numerical Modeling, Applications to Industry and Their Impact on the Human Health, pp. 73-92, 2018.

[9] Legowo, B., Bella, Y.F., Purwanto, H., Suryanto, W. & Purnama, B., *Preliminary Study of Magnetic Susceptibility on Fine Sediment Bengawan Solo River,* In Journal of Physics: Conference Series, **1951**(1), 012058, 2020.

[10] Kissel, C., Liu, Z., Li, J. & Wandres, C., *Magnetic Minerals in Three Asian Rivers Draining into the South China Sea: Pearl, Red, and Mekong Rivers,* AGU Publications, **17**(5), pp. 1678-1693, 2016.

[11] Karbassi, A.R. & Shankar, R., *Magnetic Susceptibility of Bottom Sediments and Suspended Particulates from Mulki-Pavanje River, Estuary and Adjoining Shelf, West Coast of India,* Journal of Geophysical Research Atmospheres, **99**(C5), pp. 10207-10220, 1994.

[12] Brasseur, B., Sémah, F., Sémah, A.M. & Djubiantono, T., *Pedo-sedimentary Dynamics of the Sangira Dome Hominid Bearing Layers (Early to Middle Pleistocene, Central Java, Indonesia): A Paleopedological Approach for Reconstructing, Pithecantropus (Javanese Homo Erectus) Paleoenvironment,* Quarternary International, **376**, pp. 84-100, 2015.

[13] Egli, R., Florindo, F. & Roberts, A.P., *Introduction to 'Magnetic Ironminerals in Sediments and Their Relation to Geologic Processes,*

Climate, and the Geomagnetic Field', Global and Planetary Change, **110**, pp. 259-263, 2013.

[14] Kayvantash, D., Cojana, I., Kissel, C. & Franke, C., *Magnetic Fingerprint of the Sediment Load in a Meander Bend Section of the Seine River (France)*, Geomorphology, **286**, pp. 14-26, 2017.

[15] Ayoubi, S. & Adman, V., *Iron Mineralogy and Magnetic Susceptibility of Soils Developed on Various Rocks in Western Iran,* Clay and Clay Minerals, **67**(3), pp. 217-227, 2019.

[16] Bemmelen, R.W., *The Geology of Indonesia: General Geology of Indonesia and Adjacent Archipelagoes*, Government Printing Office The Hague, Utrecht, 1949.

[17] Toha, B. & Sudarno, I. *Geological Map of the Surakarta - Giritontro Quadrangles, Jawa - Indonesia,* Geological Research and Development Center, Bandung, 1992.

[18] Zubieta, E., Larrasoaña, J.C., Aldaz, A., Casalí, J. & Giménez, R., *Assessment of Magnetite as a Magnetic Tracer for Sediments in the Study of Ephemeral Gully Erosion: Conditioning Factors of Magnetic Susceptibility*, Earth Surf Process Landforms, **46**(6), pp. 1103-1110, 2021.

[19] Chu, N., Yang, Q., Liu, F., Luo, X., Cai, H., Yuan, L. ... & Li, J., *Distribution of Magnetic, Properties of Surface Sediment and its Implications on Sediment Provenance and Transport in Pearl River Estuary,* Marine Geology, **424**, pp. 1-12, 2020.

[20] Wang, F., Zhang, W., Nian, X., Roberts, A.P., Zhao, X., Shang, Y. ... & Dong, Y., *Magnetic Evidence for Yellow River Sediment in the Late Holocene Deposit of the Yangtze River Delta, China,* Marine Geology, **427**, pp. 1-12, 2020.

[21] Hrouda, F., Chlupáčová, M. & Chadima, M., *The use of Magnetic Susceptibility of Rock in Geological Exploration,* Terrplus Geophysical Equipment Supplier, Canada, 2009.

[22] Zulaikah, S. & Nurlaily, I.P., *Magnetic Domain Distribution Analysis of Volcanic Material from the 2017 Eruptions of Mount Agung, Indonesia,* in International Conference on Mathematics, Science, and Education, Semarang, Indonesia, **1093**(1), 012029, 2018.

[23] Pratama, A., Bijaksana, S., Abdurrachman, M. & Santoso, N.A., *Rock Magnetic, Petrography, and Geochemistry Studies of Lava at the Ijen Volcanic Complex (IVC), Banyuwangi, East Java, Indonesia,* Geosciences, **8**(5), pp. 1-14, 2018.

[24] Zulaikah, S., Pujiastuti, R. & Afrillah, G.A., *Detecting Coastal Atmosphere Weathering Process on Andesite Rock Using Magnetic Susceptibility and Fe3O4/Fe2O3 Ratio,* Bulletin of the Marine Geology, **35**(1), pp. 35-40, 2020.

[25] Biedermann, A.R., *Magnetic Anisotropy in Single Crystals: A Review*, Geosciences **8**(8), 302, 2018.

[26] Yunginger, R., Bijaksana, S., Dahrin, D., Zulaikah, S., Hafidz, A., Kirana, K.H., Sudarningsih, Mariyanto & Fajar, S.J., *Lithogenic and Anthropogenic Components in Surface Sediments from Lake Limboto as Shown by Magnetic Mineral Characteristics, Trace Metals and REE Geochemistry*, Geosciences, **8**(4), 116, 2018.

[27] Vasiliev, A., Gorokhova, S. & Razinsky, M., *Technogenic Magnetic Particles in Soils and Ecological–Geochemical Assessment of the Soil Cover of an Industrial City in the Ural, Russia,* Geosciences, **10**(11), 443, 2020.

[28] Nishio, I., Morishita, T., Szilas, K., Pearson, G., Tani, K.I., Tamura, A. ... & Guotana, J.M., *Titanian Clinohumite-Bearing Peridotite from the Ulamertoq Ultramafic Body in the 3.0 Ga Akia Terrane of Southern West Greenland*, Geosciences, **9**(4), 153, 2019.

[29] Mathieu, L., *Origin of the Vanadiferous Serpentine–Magnetite Rocks of the Mt. Sorcerer Area, Lac Doré Layered Intrusion, Chibougamau, Québec*, Geosciences, **9**(3), 110, 2019.

[30] Chiarenzelli, J. R., Lupulescu, M.V., Regan, S. P. & Singer, J.W., *Age and Origin of the Mesoproterozoic Iron Oxide-Apatite Mineralization, Cheever Mine, Eastern Adirondacks, NY,* Geosciences, **8**(9), 345, 2018.

[31] Robustelli Test, C., Festa, A., Zanella, E., Codegone, G. & Scaramuzzo, E., *Distinguishing the Mélange-Forming Processes in Subduction-Accretion Complexes: Constraints from the Anisotropy of Magnetic Susceptibility (AMS)*, Geosciences, **9**(9), 381, 2019.

[32] Atarita, F.R., Bijaksana, S., Dari, N.R.D.W., Pratama, A., Taqwantara, R.F., Fajar, S.J. & Latief, F.D.E., *Anisotropy of Magnetic Susceptibility and Preferred Pore Orientation in Lava Flow from the Ijen Volcanic Complex, East Java, Indonesia*, Geosciences, **9**(7), 304, 2019.

[33] Grison, H., Petrovsky, E. & Hanzlikova, H., *Assessing Anthropogenic Contribution in Highly Magnetic Forest Soils Developed on Basalts using Magnetic Susceptibility and Concentration of Elements,* CATENA, **206**, 105480, 2021.

[34] Grison, H., Petrovsky, E., Kapicka, A. & Hanzlikova, H., *Detection of the Pedogenic Magnetic Fraction in Volcanic Soils Developed on Basalts using Frequency-Dependent Magnetic Susceptibility: Comparison of Two Instruments*, Geophysical Journal International, **209**(2), pp. 654-660, 2017.

[35] Szuszkiewicz, M., Grison, H., Petrovský, E., Szuszkiewicz, M.M., Gołuchowska, B. & Łukasik, A., *Quantification of Pedogenic Particles Masked by Geogenic Magnetic Fraction*, Scientific Reports, **11**(1), 14800, 2021.

[36] Matasova, G.G., Kazansky, A.Y., Shchetnikov, A.A., Filinov, I.A., Berdnikova, N.E. & Berdnikov, I.M., *Sedimentation and Environmental Dynamics of the Tunka Rift Valley (Baikal Region) in the Late Pleistocene-Holocene Based on the Analysis of Lithological and Rock Magnetic*

Properties of the Deposits from Upper Paleolithic Sites, Archaeological Research in Asia, **26**, 100266, 2021.

[37] Liu, Q., Sun, Y., Qiang, X., Tada, R., Hu, P., Duan, Z.Z., Jiang, Z., Liu, J. & Su, K., *Characterizing Magnetic Mineral Assemblages of Surface Sediments From Major Asian Dust Sources and Implications for the Chinese Loess Magnetism,* Earth, Planets and Space, **67**(1), pp. 1-17, 2015.

[38] Li, M., Zhu, S., Ouyang, T., Tang, J. & Tang, Z., *Magnetic Properties of the Surface Sediments in the Yellow River Estuary and Laizhou Bay, Bohai Sea, China: Implications for Monitoring Heavy Metals,* Journal of Hazardous Materials, **410**, 124579, 2021.

[39] Bijaksana, S., Huliselan, E., Safiuddin, L.O., Fitriani, D., Tamuntuan, G. & Agustine, E., *Rock Magnetic Methods in Soil and Environmental Studies: Fundamentals and Case Studies,* Procedia Earth and Planetary Science, **6**, pp. 8-13, 2013.

[40] Wang, B., Zhang, X., Zhao, Y., Zhang, M. & Jia, J., *Spatial and Temporal Distribution of Pollution Based on Magnetic Analysis of Soil and Atmospheric Dustfall in Baiyin City, North Western China,* International Journal of Environmental Research and Public Health, **18**(4), 1681, 2021.

[41] Maity, R., Venkateshwarlu, M., Mondal, S., Kapawar, M.R.D., Gain & Paul, P., *Magnetic and Microscopic Characterization of Anthropogenically Produced Magnetic Particles: a Proxy for Environmental Pollution,* International Journal of Environmental Science and Technology, **18**, pp. 1793-1808, 2021.

[42] Scheidt, S., Egli, R., Lenz, M., Rolf, C., Fabian, K. & Melles, M., *Mineral Magnetic Characterization of High-Latitude Sediments From Lake Levinson-Lessing, Siberia,* Geophysical Research Letters, **48**(10), e2021GL093026, 2021.

[43] Warrier, A.K., Mahesh, B.S., Mohan, R. & Shankar, R.A., *43-Ka Mineral Magnetic Record of Environmental Variations from Lacustrine Sediments of Schirmacher Oasis, East Antarctic,* CATENA, **202**, 105300, 2021.

[44] Rawat, S., Gupta, A.K., Srivastava, P., Sangode, S.J. & Nainwal, H.C., *A 13,000 Year Record of Environmental Magnetic Variations in the Lake and Peat Deposits from the Chandra Valley, Lahaul: Implications to Holocene Monsoonal Variability in the NW Himalaya,* Palaeogeography, Palaeoclimatology, Palaeoecology, **440**, pp. 116-127, 2015.

[45] Grison, E. Petrovsky, H., Kapicka, A. & Hanzlikova, H., *Detection of the Pedogenic Magnetic Fraction in Volcanic Soils Developed on Basalts using Frequency-Dependent Magnetic Susceptibility: Comparison of Two Instruments,* Geophysical Journal International, **209**(2), pp. 654-660, 2017.

[46] Hunt, C.P., Moskowitz, B.M. & Banerjee, S.K., *Magnetic Properties of Rocks and Minerals,* American Geophysical Union, **3**, pp. 189-203, 1995.

[47] Strehlau, J.H., Hegner, L.A., Strauss, B.E., Feinberg, J.M. & Penn, R.L., *Simple and Efficient Separation of Magnetic Minerals from Speleothems*

and Other Carbonates, Journal of Sedimentary Research, **84**(11), pp. 1096-1106, 2014.

[48] Habibi, N., *Preparation of Biocompatible Magnetite-Carboxymethyl Cellulose Nanocomposite: Characterization of Nanocomposite by FTIR, FESEM and TEM*, Spectrochimica Acta Part A: Molecular and Biomolecular Spectroscopy, **131**, pp. 55-58, 2014.

[49] Amiri, S. & Shokrollahi, H., *Magnetic and Structural Properties of RE Doped Co-Ferrite (RE=Nd, Eu, and Gd) Nano-particles Synthesized by co-Precipitation*, Journal of Magnetism and Magnetic Materials, **345**, pp. 18-23, 2013.

[50] Hrouda, F., Pokorný, J., Ježek, J. & Chadima, M., *Out-of-Phase Magnetic Susceptibility of Rocks and Soils: a Rapid Tool for Magnetic Granulometry*, Geophysical Journal International, **194**(1), pp. 170-181, 2013.

[51] Patriadi, A., Soemitro, R.A.A. & Warnana, D.D., *Preliminary Assessment to Sediment Evaluation the Estuary of Bengawan Solo River*, in Proceeding of Soft Soils, Bandung, 2016.

[52] Fiantis, D., Nelson, M., Van Ranst, E., Shamshuddin, J. & Qafoku, N.P., *Chemical Weathering of New Pyroclastic Deposits from Mt. Merapi (Java), Indonesia*, Journal of Mountain Science, **6**(3), pp. 240-254, 2009.

[53] Ilham, D.J., Kautsar, F.R., Januarti, J., Anggarini, U. & Fiantis, D., *The Potential use of Volcanic Deposits for Geopolymer Materials*, in International Conference of Bio-Based Economy and Agricultural Utilization, Andalas, **497**(1), 0120352020, 2020.

[54] Mhashhash, A., Bockelmann-Evans, B. & Pan, S., *Effect of Hydrodynamics Factors on Sediment Flocculation Processes in Estuaries*, Journal Soil Sediment, **18**, pp. 3094-3103, 2018.

[55] Salama, W., El Aref, M. & Gaupp, R., *Spectroscopic Characterization of Iron Ores Formed in Different Geological Environments using FTIR, XPS, Mössbauer Spectroscopy and Thermoanalyses*, Spectrochimica Acta Part A: Molecular and Biomolecular Spectroscopy, **136**, pp. 1816-1826, 2015.

[56] Nurcholis, M., DF Yudiantoro, D.F., Haryanto, D., AB Dianputra, A.B. & K Aji, K.A., *Process and Mineralogy of Volcanic Materials on The South Side of The Old Lawu Volcano in Java Island*, Journal of Soil Science and Agroclimatology, **16**(2), pp. 127-138, 2019.

[57] Maxbauer, D.P., Feinberg, J.M., Fox, D.L. & Clyde, W.C., *Magnetic Minerals as Recorders of Weathering, Diagenesis, and Paleoclimate: A Core–Outcrop Comparison of Paleocene–Eocene Paleosols in the Bighorn Basin, WY, USA*, Earth and Planetary Science Letters, **452**, pp. 15-26, 2016.

[58] Harrison, R.J., Dunin-Borkowski, R.E., Kasama, T., Simpson, E.T. & Feinberg, J.M., *Magnetic Properties of Rocks and Minerals*, Treatise on Geophysics, **1-10**, pp. 579-630, 2015.

[59] Legowo, B., Putra, S. Mufti, M.K., Purwanto, H., Rifai, H., Suryanto, W. & Purnama, B., *Identification Pyroclastic Flow of Magnetic Minerals (Holocene Volcano): A Case Study of Paleo-Volcano Lawu on the South Side, Central Java, Indonesia,* Kuwait Journal of Science, **50**(4), pp. 724-730, 2023.

[60] Kim, W., Doh, S.J., Park, Y.H. & Yun, S.T., *Two-Year Magnetic Monitoring in Conjunction with Geochemical and Electron Microscopic Data of Roadside Dust in Seoul, Korea,* Atmos. Environ, **41**(35), pp. 7627-7641, 2007.

[61] Lu, S.G., Chen, Y.Y., Shan, H.D. & Bai, S.Q., *Mineralogy and Heavy Metal Leachability of Magnetic Fractions Separated from Some Chinese Coal Fly Ashes,* J. Hazard, Mater, **169**(1-3), pp. 246-255, 2009.

[62] Wang, X.S. & Qin, Y., *Magnetic Properties of Urban Topsoils and Correlation with Heavy Metals: A Case Study from The City of Xuzhou, China,* Environ, Geol, **49**, pp. 897-904, 2006.